DETERMINATION OF MAGNETIC BEARING POWER LOSSES VIA PARAMETER ESTIMATION

L. Scott Stephens
Carl R. Knospe
Center For Magnetic Bearings
University of Virginia
Charlottesville, Virginia, U.S.A.

ABSTRACT

The most common and accurate magnetic bearing power loss estimation technologies consist of laboratory test rigs which utilize spin-down data or dynamometer data to compute the losses. However, these technologies do not lend themselves to effective determination of core power losses arising in field machines. An on-line method that could be used for existing bearings in field machines would be beneficial to both end-users and equipment manufacturers. In this paper, a method of this kind is presented which requires only temperature data to compute the losses. This method uses a sequential parameter estimation technique to reduce the data. The new method is applied to a high speed experimental apparatus to estimate power losses at various combinations of rotational speed and coil currents. These power losses are due to windage, coil ohmic heating, eddy currents due to ripple from switching amplifiers, and journal rotation in the magnetic field. Results using the new method are presented for two different bearings: a silicon iron design and a cobalt iron design. Combined eddy current and hysteresis losses have been determined for speeds up to 3.1 million DN (mm-rpm) and flux densities just below saturation for each bearing. To the authors' knowledge, this is the first accounting of core loss in cobalt iron at high speeds.

INTRODUCTION

As potential applications continue to be identified, magnetic bearings are being applied in increasingly hostile environments with ever tougher performance requirements. High speed machines where surface speeds exceed several million DN are a demanding application of magnetic bearings. With greater surface speed comes greater material stress and rotating power losses which threaten the mechanical integrity and performance of the machine.

Present day field testing consists of spin down tests that yield a bulk rotational power loss. This bulk loss contains hysteresis, eddy currents, windage, unbalance torque and torque due to seals, which normally cannot be separated [2]. So far, detailed power loss prediction for magnetic bearings has been confined to the laboratory where well established methods are implemented. These include: (1) Epstein tests [13] and (2) Rowland ring tests[1] for determination of alternating hysteresis loss and eddy current loss in test samples, (3) spin-down tests of a magnetic bearing supported rotor conducted in a vacuum chamber [15] and (4) dynamometer tests which determine core losses separated from windage losses. These tests are very accurate in measuring core losses in test specimens or test bearings but their results are not easily translated to existing field machines where bearing properties may vary.

This paper presents a method to predict power losses in laboratory or field machines, and shows the results of applying this method to estimate losses on an experimental apparatus. The method is a model based, sequential parameter estimation which utilizes temperature measurements to construct a solution. The parameters are estimated via a non-linear, least squares smoothing technique and include initial temperatures, unknown convection coefficients and power losses. Important results for the experimental apparatus include new core loss estimates for two bearings at speeds up to 3.1 million DN and coil currents that approach saturation.

EXPERIMENTAL APPARATUS DESCRIPTION

Figure 1 shows a schematic diagram of the experimental apparatus used. The apparatus consists of a shaft supported by two ball bearings at each end and driven by an air turbine. The ball bearing closest to the driver is termed the inboard bearing and that furthest from the driver is termed the outboard bearing. A single magnetic bearing is located at the midspan of the shaft and a constant bias current is supplied to each stator coil by use of a switching amplifier. This generates a magnetic field in which the magnetic bearing journal is held centered via the ball bearings. When the journal rotates in the magnetic field, core losses are produced.

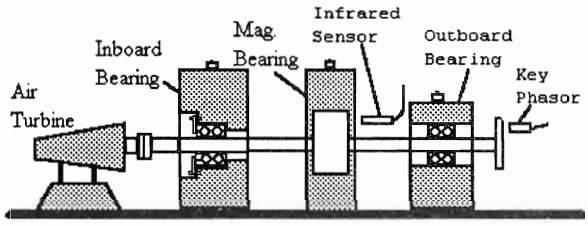

FIGURE 1: Schematic of Experimental Apparatus

Four temperature measurements are made directly on the apparatus and are recorded by a computer via a data acquisition board. Three of the measurements are made by regular type "K" thermocouples and consist of the inboard ball bearing housing, the outboard ball bearing housing and the back iron of the magnetic bearing stator. A non-contacting infrared temperature probe is used to provide the fourth measurement, the temperature of the magnetic bearing journal. The ambient air temperature is also periodically recorded. A key phasor is used to obtain and display the rotational speed which can be changed as needed by an operator using a manual air flow valve. Two magnetic bearings of different materials and designs were tested. Table 1 gives the geometry and construction of the test bearings.

TABLE 1: Test Bearing Construction

Property	Bearing 1	Bearing 2
Material	Silicon Iron	Cobalt Iron
Journal O.D.	58.4 mm (2.3")	76.2 mm (3.0")
Journal I.D.	19.1 mm (0.75")	19.1 mm (0.75")
Journal Length	25.4 mm (1.0")	25.4 mm (1.0")
Journal Mass	0.50 kg (1.1 LB)	0.86 kg (1.9 LB)
Radial Gap Length	0.64 mm (0.025")	0.25 mm (0.010")
Journal Lam. Thickness	0.18 mm (0.007")	0.15 mm (0.006")
Insulation Coating	C5	Oxide
# of Poles	8	8

Thermal Modeling Of Experimental Apparatus

As with any model based parameter estimation method, the main disadvantages are the sensitivity of the estimates to erroneous a priori models of the apparatus and the inherent computational burden required to make the estimates [5]. Unfortunately, these disadvantages are trade offs between one another. If too complex a model is chosen, the computational burden becomes unbearable. However, if too simple a model is chosen, it doesn't represent the apparatus closely enough and the estimates are poor. Clearly, the strength of the parameter estimation results rests on the validity of the assumed model. For the results presented here, the experimental apparatus was modeled as fifteen lumped thermal masses and was assumed to be axisymmetric. The following are the assumptions used in generating the thermal model:

i. Lumped thermal masses
ii. Two-dimensional, axisymmetric model
iii. Bulk conductivity used for pole/coil region
iv. Air gap thermal resistance is negligible
v. A minimum number of convection coefficients are used to describe the boundary conditions
vi. No heat is lost axially across the coupling to the air turbine
vii. Key phasor disk is thermally negligible

Modeling the apparatus using lumped thermal masses is valid as long as the ratio of conductive thermal resistance to convective thermal resistance is sufficiently small [12]. This ratio is the non-dimensional Biot number, B_i, and the usually accepted threshold for use of lumped mass models is as follows [6] [7] [12]:

$$B_i = \frac{hL}{K} < 0.1 \qquad (1)$$

Where, h is the convection coefficient, L is the characteristic length and K is the thermal conductivity. Essentially, this means that the temperature of each lumped mass is constant throughout at any time.

With these assumptions, first order differential equations for each lumped mass can be written and assembled in the following matrix differential equation:

$$\dot{\underline{T}}(t) = A(\underline{h}, K_b, t)\underline{T}(t) + T_f \underline{B}_f(\underline{h}) + B_q \underline{Q} \qquad (2)$$

where $\underline{T}(t)$ is the state vector containing the temperatures of each thermal mass, $A(\underline{h}, K_b, t)$ is the model dynamics matrix, $\underline{h}$ is the column vector

containing the convection coefficients, K_b is the bulk thermal conductivity of the pole/coil region, T_f is the ambient air temperature, $\underline{Q}$ is the vector containing the power losses to be estimated, and $\underline{B}_f(\underline{h})$ and B_q are the input vector and matrix, respectively.

Parts of the thermal model given by equation (2) are completely known and others are only known to be constant under certain conditions; hence their amplitudes must be estimated. The parameters that must be estimated are the convection coefficients, $\underline{h}$, bulk thermal conductivity, K_b, initial temperatures of the lumped masses, $\underline{T}_o$, and the power losses, $\underline{Q}$. This results in a total of 25 parameters to estimate. Fortunately, if a properly selected thermal cycle is applied to the test apparatus, then subsets of these parameters may be estimated sequentially. This procedure reduces the number of parameters in any one estimation and increases the accuracy of the estimates.

PARAMETER ESTIMATION

Non-Linear Smoothing via Least Squares

Examining equation (2) it is evident that the estimated parameters appear nonlinearly. Therefore, in order to apply the method of least squares to perform the parameter estimates, the problem must be rewritten using an augmented state vector, $\underline{X}$, and linearized about a nominal state trajectory, $\underline{X}^*$, via a Taylors series expansion. The state space representation of the augmented system is written as:

$$\dot{\underline{X}}(t) = \begin{bmatrix} \dot{\underline{T}}(t) \\ \dot{\underline{h}} \\ \dot{K}bk \\ \dot{\underline{Q}} \end{bmatrix} = \begin{bmatrix} A(\underline{h}, Kbk, t)\underline{T}(t) + T_f \underline{B}_f(h) + B_q \underline{Q} \\ \underline{0} \\ 0 \\ \underline{0} \end{bmatrix} = \begin{bmatrix} \underline{F}_1(\underline{X}, t) \\ \underline{0} \\ 0 \\ \underline{0} \end{bmatrix} \quad (3a)$$

$$\underline{Y}(t) = C\underline{X}(t) + \underline{\varepsilon} \quad (3b)$$

where $\underline{Y}(t)$ is the output vector of measurements, $\underline{\varepsilon}$ is the vector of measurement errors and the matrix C selects the temperatures where measurements are taken. Since the unknown parameters are known to be constant for a given running condition, they can be determined by estimating only the initial condition of the augmented state vector, $\underline{X}_0$. Such a parameter estimation is termed an optimal smoothing [5]. Performing the Taylors Series expansion, equations (3) are written as:

$$\dot{\underline{X}}(t) = \underline{F}(\underline{X}^*(t), t) + \left[\frac{\partial \underline{F}}{\partial \underline{X}}\right]_{\underline{X}=\underline{X}^*} (\underline{X} - \underline{X}^*) + H.O.T. \quad (4a)$$

$$\underline{Y}^*(t) = C\underline{X}^*(t) + \underline{\varepsilon} \quad (4b)$$

where $\underline{X}^*(t)$ and $\underline{Y}^*(t)$ are the nominal state trajectory and nominal output trajectory of the non-linear system, respectively. The system is amenable to a least squares parameter estimation if written in terms of error states, $\underline{e}_x$, and the measurement residual, $\underline{e}_y$, which are defined as follows:

$$\underline{e}_x = \underline{X} - \underline{X}^* \quad (5a)$$

$$\underline{e}_y = \underline{Y} - \underline{Y}^* \quad (5b)$$

In terms of these variables the thermal model of the experimental apparatus is then written as [14]:

$$\dot{\underline{e}}_x = \left[\frac{\partial \underline{F}}{\partial \underline{X}}\right]_{\underline{X}=\underline{X}^*} \underline{e}_x \quad (6a)$$

$$\underline{e}_y = C\underline{e}_x + \underline{\varepsilon} \quad (6b)$$

Equations (6) compose a linear time variant system. The systems response to initial conditions is given as follows [4]:

$$\underline{e}_y = C\Phi(t, t_o)\underline{e}_{xo} + \underline{\varepsilon} \quad (7)$$

where $\underline{e}_{xo}$ is the initial condition of the error state vector, $\underline{e}_x$, and $\Phi(t, t_o)$ is the state transition matrix. The state transition matrix is computed by noting that it satisfies equation (6a) and can be integrated ahead in time with the identity matrix used as the initial condition. Least squared smoothing techniques can then be applied directly to the error model in equations (6) by using the solution given in equation (7) at each time step in which measurements are taken. In this manner, a solution is constructed using all available measurements. Equation (7) then becomes the following:

$$\begin{bmatrix} \underline{e}_{y1} \\ \underline{e}_{y2} \\ \cdot \\ \cdot \\ \underline{e}_{ym} \end{bmatrix} = H\underline{e}_{xo} + \begin{bmatrix} \underline{\varepsilon}_1 \\ \underline{\varepsilon}_2 \\ \cdot \\ \cdot \\ \underline{\varepsilon}_n \end{bmatrix} \quad (8a)$$

$$H = \begin{bmatrix} C\Phi_1(t,t_o) \\ C\Phi_2(t,t_o) \\ \cdot \\ \cdot \\ C\Phi_n(t,t_o) \end{bmatrix} \quad (8b)$$

where n is the total number of measurements taken. For a least squares smoothing, the performance index is defined as the minimum squared measurement error. Therefore, the estimated parameters minimize the following:

$$J = \underline{\varepsilon}^T \underline{\varepsilon} \quad (9)$$

The least squares solution is obtained by substituting equations (8) into (9) and utilizing a singular value decomposition (SVD) methodology. If the SVD of H is UWV^T, then the least squares estimate is given as [10]:

$$\underline{\hat{e}}_{xo} = \sum_{j=1}^{m} \left(\frac{U_j^T \cdot \underline{e}_y}{w_j}\right) V_j \quad (10)$$

where m is the number of estimated parameters, U_j and V_j are the columns of U and V, and w_j are the diagonal entries of W (the singular values). The actual parameter estimates are then simply given by:

$$\underline{\hat{X}}_0 = \underline{\hat{e}}_{xo} + \underline{X}_o^* \quad (11)$$

Where $\underline{X}_o^*$ is the initial condition of the nominal state trajectory, $\underline{X}^*$.

Sequential Estimation Technique

Given the non-linear optimal smoothing procedure described above, estimates of the different unknown thermal parameters of the experimental apparatus can be made sequentially. This is done by running the apparatus through a simple thermal cycle consisting of four distinct steps. In each step some of the parameters are unknown while others are known to be zero for the given operating conditions. In this manner, different loss mechanisms are separated from one another via a sequence of estimations. Also, the estimation accuracy is increased because the number of estimations at any one time is minimized. Figure 2, shows a typical temperature profile for the experimental apparatus resulting from the four step thermal cycle. The experimental data is shown along with curves resulting from a simulation based on the model of the apparatus with the "best-fit" set of parameters.

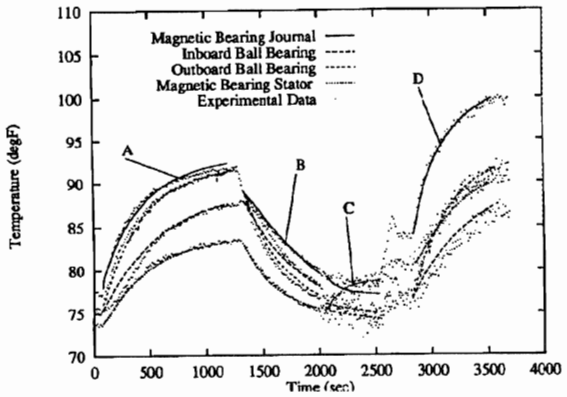

FIGURE 2: Four Step Temperature Profile

The four steps of the cycle are described as follows:

A. Coil current = 0; rotor speed constant
B. Coil current = 0; rotor speed =0 (free decay)
C. Coil current constant; rotor speed = 0
D. Coil current constant; rotor speed constant

In each step of the thermal cycle different unknown parameters are estimated. In step A, the ball bearing power losses and windage loss is estimated while the eddy current, hysteresis and coil ohmic/stator switching losses are known to be zero. In step B, the convection coefficients are determined. In step C the coil ohmic and stator switching losses are estimated while all rotating losses are known to be zero. Finally, in step D, the combined eddy current and hysteresis loss in the rotating journal is determined for the particular operating condition (speed and coil current).

As stated previously, the main disadvantage of using this method in comparison to vacuum spin down or dynamometer tests is the greater uncertainty in the power loss estimates. However, several advantages can be seen immediately. First the method can be adapted to *any* machine in the field or in the laboratory. Thus power loss estimates can be made on existing field equipment. Second, the method can differentiate between windage loss and other core losses without having to run the rotor in a vacuum. This is an advantage for high speed testing where the journal core losses can generate very high temperatures on a magnetically supported rotor in a vacuum. High journal temperature may reduce rotating losses as the lamination resistance increases with temperature. Also, high temperatures will decrease the bearing clearance affecting the magnetic field. Last, high journal temperatures can threaten the mechanical integrity of the rotating component, especially interference fits.

EXPERIMENTAL RESULTS AND DISCUSSION

Tests were made of the two magnetic test bearings for speeds between 10 and 50 thousand rotations per minute (Krpm) and for bias current levels between 0.4 and 2.0 amperes. For each speed/ampere combination the apparatus was cycled through the four thermal conditions as described above. Each set of resulting temperature profiles was then used in the parameter estimation procedure to determine the unknown power losses of the apparatus. Figure 3 shows the estimated power loss due to windage for the two test bearings at the various speeds.

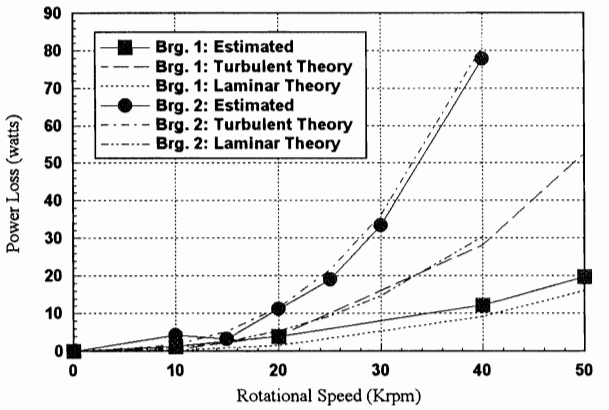

FIGURE 3: Windage Losses

As in ref. [15], which computes losses via the classical spin-down vacuum chamber method, the windage losses are compared to theoretical predictions based on Karmans coefficients of resisting moment and assuming either a turbulent or laminar boundary layer. The windage loss around a rotating journal can be approximated by disk type losses and cylinder type losses. The equations governing the windage loss for a cylinder and a disk are given below [11].

Cylinder:

$$P_{loss} = \frac{\pi}{2} C_m \rho R^4 L \omega \qquad (12a)$$

where: $C_m = 3.460(\mathrm{Re})^{-0.5}$ (Laminar)

$= 0.146(\mathrm{Re})^{-0.2}$ (Turbulent)

Disk:

$$P_{loss} = \frac{1}{4} C_m \rho R^5 \omega^3 \qquad (12b)$$

where: $C_m = 3.870(\mathrm{Re})^{-0.5}$ (Laminar)

$= 0.146(\mathrm{Re})^{-0.2}$ (Turbulent)

where C_m is the coefficient of resisting moment, ρ is the density of air, R is the radius of the journal, L is the journal length, ω is the rotational speed, and Re is the Reynolds number. The Reynolds numbers for a spinning cylinder and a spinning disk are given below.

$$\mathrm{Re} = \frac{2\pi R L \omega}{\nu} \quad \text{(Cylinder)} \qquad (13a)$$

$$\mathrm{Re} = \frac{\omega R^2}{\nu} \quad \text{(Disk)} \qquad (13b)$$

For Bearing 1, the estimated windage loss data closely follows the laminar assumption. Examination of the Reynolds number for this bearing shows it to be in the laminar or transition region ($\mathrm{Re}<5e^5$) for the disk type losses at all speeds and also for the cylinder type losses at speeds less than 18 Krpm. This explains why Bearing 1 follows the loss curve based on a laminar flow assumption. For Bearing 2, the estimated windage loss data closely follows the turbulent assumption. Examining the Reynolds number for Bearing 2 reveals it to be in the turbulent regime for the disk type losses at speeds greater than 27 Krpm and also for the cylinder type losses at all speeds of interest. This explains why Bearing 2 follows the turbulent flow assumption. The authors view the close agreement of the estimated windage losses for the two bearings with the theoretical losses as confirmation of the estimation technique used.

Figure 4 shows the estimated power loss due to stator switching and coil ohmic losses at the different coil currents for each of the two bearings.

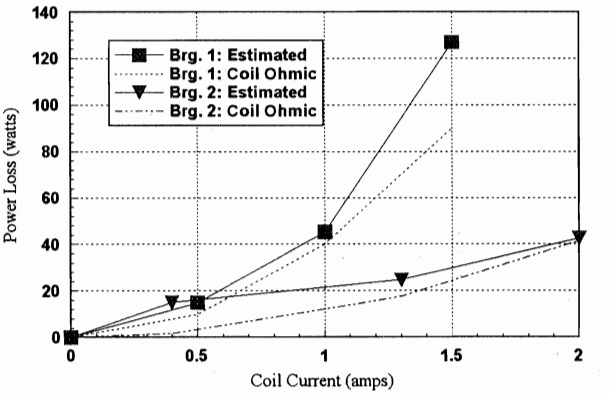

FIGURE 4: Coil Ohmic and Stator Switching Losses

The coil ohmic losses and stator switching losses (due to alternating hysteresis in the stator) cannot be separated by the proposed method. The estimate of these combined losses is compared to the actual coil

ohmic losses determined by directly measuring the current and resistance of each coil and calculating i^2R. The coil resistance in Bearing 1 was much greater than that in Bearing 2 as the figure indicates. Note that for Bearing 2, the estimated combined loss is very close to the actual coil ohmic loss while for Bearing 1, the estimates exceed the ohmic loss. Recall that Bearing 1 has a non-laminated stator where Bearing 2 has a laminated one. Therefore, we would expect a higher stator switching contribution to combined losses in Bearing 1. This is confirmed by the results shown in Figure 4. Note the larger error in losses of Bearing 2 at low current. This shows the difficulty in estimating a small power loss where low temperature rises result. When the temperature rises are close to the noise level of the thermocouples then the parameter estimation cannot differentiate between the two. Hence a large error results in the estimate of a small parameter. The authors view the data presented in Figure 4 as further confirmation of the estimation technique.

Finally, Figures 5 and 6 show the estimated journal core losses for Bearings 1 and 2, respectively, at the different speed/coil current combinations.

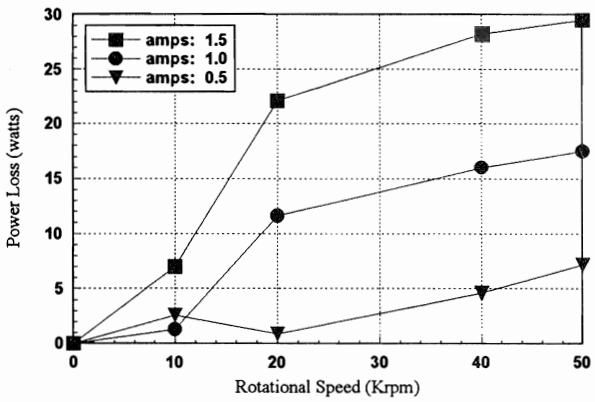

FIGURE 5: Journal Core Losses for Bearing 1

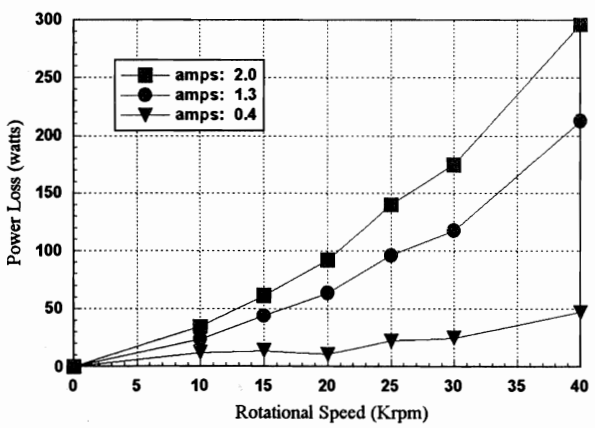

FIGURE 6: Journal Core Losses for Bearing 2

Given that the two test bearing designs are quite different, the coil currents result in different flux densities for each. Also, at high rotational speeds the flux densities may be different than at zero speed due to lamination radial growth and eddy current skin effects. These two effects are discussed later. Table 2 gives the zero speed flux densities of each test bearing at the different coil currents.

TABLE 2: Test Bearing Flux Densities

	Coil Current (Amperes)	Flux Density (Tesla)
Bearing 1	0.5	0.3
	1.0	0.6
	1.5	0.9
Bearing 2	0.4	0.3
	1.3	0.9
	2.0	1.5

The core loss magnitudes in Figures 5 and 6 are quite different for each test bearing. The core losses in Bearing 1 are less than 30 watts for all running conditions and those for Bearing 2 are less than 300 watts for all running conditions. The two bearing designs are different in many aspects so a one-to-one comparison of the losses based only on material differences is not a valid one. However, the manufacturers published data for alternating current losses in silicon iron and cobalt iron showed losses of the same order as those estimated in Figures 5 and 6 for each bearing.

Many references have reported the shape of the journal core loss curves vs. speed to be closely quadratic [8] [15]. This shape is suggested by the classical formula for the eddy current portion of the losses which is found in reference [13] as:

$$P_{ec} = \frac{\pi^2 f^2 \tau^2 B_{\max}^2}{6\rho} \qquad (14)$$

where f is the frequency, $B_{\max}$ is the maximum flux density, σ is the resistivity, and τ is the lamination thickness. In the case of Bearing 1, Figure 5 indicates that the power loss curves do not follow the classical quadratic shape suggested in equation (14) as the curves tend to roll over at higher speed. However, for Bearing 2, Figure 6 indicates a closer adherence of the data to the classical behavior. Two effects which are neglected in the classical theory but become important at high speeds are the eddy current skin effect and decrease of the radial air gap. These two effects tend to cancel as the former decreases losses and the latter

increases losses. The nature of the curves in Figures 5 and 6 may be explained by these two phenomena.

The eddy current skin effect tends to retard losses due to a back magnetomotive force (MMF) which is generated at high speeds. A more complete form of the classical eddy current loss equation which includes the back MMF term is as follows [13]:

$$P_{ec} = \frac{\pi^2 f^2 \tau^2 B_{\max}^2}{6\sigma}\left[1 - \frac{6}{945}(\alpha d)^4 \cdots\right] \qquad (15)$$

$$\alpha d = \pi\tau\sqrt{\frac{2\mu f}{\sigma}}$$

where μ is the permeability and all other variables are defined above. As an indication of the effect of the eddy current skin effect in an ideally laminated journal, the effect of the αd term on equation (15) must be examined. If $\alpha d \approx 1$, then the back MMF term is negligible and equation (15) reduces to the classical eddy current equation (14). However when $\alpha d > 1$, the back MMF term may not be neglected. Bearings 1 and 2 are equally as likely to experience the eddy current skin effect as $\alpha d = .02\sqrt{f}$ for each. Then for frequencies greater than about 10 KHz the back MMF in equation (15) becomes important for both bearings. Reference [8] suggests that the proper frequency content for eddy current losses in magnetic bearings is two times the pole pass frequency. Based on this assumption, both test bearings will become susceptible to the skin effect only at speeds greater than about 48 Krpm. Figure 5 indicates that this is clearly not the case for Bearing 1 as it tends to roll over at much lower speeds. This suggests that at high speeds the proper frequency content is not necessarily two times the pole pass frequency. The proper frequency components to use perhaps could be determined from the spectral decomposition of the flux waveform encountered by the journal as it rotates passed poles as is examined in reference [9].

The effect of a decrease in radial air gap is to increase the flux density in the circuit for a given coil current and increase the losses accordingly. The flux density in the air gap is inversely proportional to the square of the gap length. According to classical mechanical disk theory [3], the gap lengths for each test bearing were computed at each running speed. For Bearing 1, the gap length will decrease no more than 0.7 mils at top speed. This corresponds to only a 5.6% increase in flux density. For Bearing 2, however, where the original zero speed gap is quite small, the disk growth can be as high as 1.0 mil at top speed. Consequently the flux density will increase by 23.5% for Bearing 2.

Therefore, the authors expect that in the case of Bearing 1 the eddy current skin effect dominates over the lamination growth effect and the curves roll over as seen in Figure 5. However, for Bearing 2, the authors believe that the disk growth effect is large enough to cancel out the skin effect, hence the curves have the more classical quadratic nature. Another possible cause for the different curve shapes in Figures 5 and 6 is that the bearings are not ideally laminated. Differences in inter-laminar conductivity resulting from manufacturing methods could produce significant variations in the core loss curves. For example, the insulation used between laminations is not the same for the two bearings. Differences of this kind between the two bearings could result in one test bearing being more susceptible to the eddy current skin effect than the other.

One limitation of using the proposed parameter estimation method to estimate losses is that error bars cannot be placed on the final estimates without using prohibitively intensive computational methods. However, as an indication of how accurate the final power loss results are, a comparison is made between simulated temperature profiles based on the parameter estimates and the experimental temperature profiles. Again, Figure 2 shows a typical set of simulated and experimental temperature profiles. This type of data is available for each core loss estimate. Figure 7 shows the average difference and standard deviation of the simulated and experimental profiles for loss estimates at each combination of speed and amperage for the two test bearings.

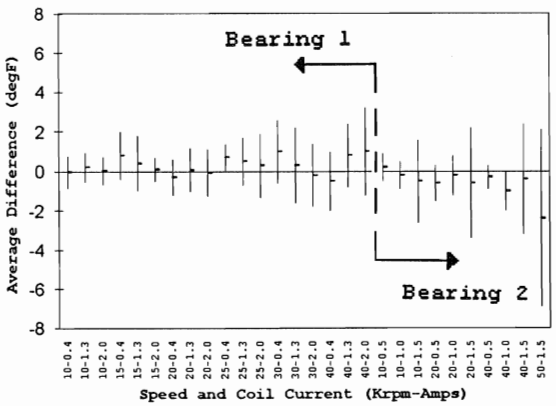

FIGURE 7: Average Difference and Standard Deviation Between Experimental and Simulated Temperature Profiles

The thermocouples are only accurate to +/1°F. Therefore the method cannot yield temperature profiles that match the experimental ones anymore accurate than this. Figure 7 indicates this to be the case.

CONCLUSIONS

Power loss data for two different bearings running at high speeds was determined experimentally using a new method to reduce temperature data. The method uses temperature measurements exclusively to determine the losses. The method can be used in laboratory test rigs or field machines. Power loss results show that at high speeds certain phenomenon that are not generally considered in the loss theory must be accounted for. Good agreement was seen between estimated windage losses and those predicted by theory. Good agreement was also seen between estimated losses due to coil ohmic and stator switching and theoretical coil ohmic losses. It was also determined that the method has difficulty determining small power losses where the temperature rises are close to the accuracy of the thermocouples. This method shows promise for both laboratory and field use. Journal core loss data was presented for silicon iron and cobalt iron magnetic bearings at speeds and coil currents not previously published.

REFERENCES

1. ASTM, "Standard Test Method for Alternating-Current Magnetic Performance of Laminated Core Specimens Using the Dieterly Bridge Method", Standard no. A346, 1988

2. Delprete, C., et. al., "High Speed Asynchronous Motor with High Tc Superconducting Bearings", Proceedings of the Third International Symposium on Magnetic Bearings, Technomic Publishing Co., 1992.

3. Den Hartog, J.P., Advanced Strength of Materials, Dover Publishing Inc., 1987.

4. Friedland, B., Modern Control Theory, Mcgraw-Hill Book Company, 1986

5. Gelb, A., Applied Optimal Estimation, The M.I.T. Press, 1974.

6. Holman, J.P., Heat Transfer, McGraw-Hill Book Co., 1986.

7. Karlekar, B.V. and Desmond, R.M., Engineering Heat Transfer, West Publishing Co., 1977.

8. Kasarda, M.E.F., et. al., Comparison of Experimentally Measured and Calculated Losses in Planar Radial Magnetic Bearings, Proceedings of the Rotating Machinery Conference, 1993

9. Matsumura, F. and Hatake, K., Relation between Magnetic Pole Arrangement and Magnetic Loss in Magnetic Bearing, Proc. of the 3rd Intl. Symposium on Magnetic Bearings, Technomic Publishing, 1992

10. Press, W.H., et. al., Numerical Recipes, Cambridge University Press, 1989.

11. Schlichting, H., Boundary Layer Theory, McGraw-Hill Book Company, 1968

12. Shearer, J.L and Kulakowski, B.T., Dynamic Modeling and Control of Engineering Systems, Macmillan Publishing Co., 1990.

13. Staff, MIT Electrical Engineering Dept., Magnetic Circuits and Transformers, John Wiley & Sons, 1945.

14. Tapley, B.D. and Born, G.H., Statistical Orbit Determination Problem, Center for Space Research, Austin, TX, 1985.

15. Ueyama, H. and Fujimoto, Y., "Iron Losses and Windy Losses of High Rotational Speed Rotor Suspended By Magnetic Bearings", Proceedings of the Second International Symposium on Magnetic Bearings, 1990.

ACKNOWLEDGMENTS

The authors wish to express their sincerest gratitude those who made this work possible. Those persons include Mr. Klaus Brun for use of the data acquisition system and the hours spent setting it up. Prof. Eric Maslen, for help with many hardware aspects and theoretical discussions. Finally, Mr. Kevin Knight for helping with the many laboratory set ups.